The first 62 AGN observed with SDSS-IV MaNGA – II. Resolved stellar populations

Nícolas Dullius Mallmann,[1,2]★ Rogério Riffel,[1,2] Thaisa Storchi-Bergmann,[1,2]
Sandro Barboza Rembold,[2,3] Rogemar A. Riffel,[2,3] Jaderson Schimoia,[1,2,3]
Luiz Nicolaci da Costa,[2] Vladimir Ávila-Reese,[4] Sebastian F. Sanchez,[4]
Alice D. Machado,[2,3] Rafael Cirolini,[2,3] Gabriele S. Ilha[2,3] and
Janaína C. do Nascimento[1,2]

[1]*Departamento de Astronomia, Universidade Federal do Rio Grande do Sul - Av. Bento Gonçalves 9500, Porto Alegre, RS, Brazil*
[2]*Laboratório Interinstitucional de e-Astronomia, Rua General José Cristino, 77 Vasco da Gama, Rio de Janeiro 20921-400, Brazil*
[3]*Departamento de Física, Centro de Ciências Naturais e Exatas, Universidade Federal de Santa Maria, 97105-900, Santa Maria, RS, Brazil*
[4]*Instituto de Astronomía, Universidad Nacional Autónoma de México, A. P. 70-264, C.P. 04510, México, D.F., Mexico*

ABSTRACT

We present spatially resolved stellar population (SP) age maps, average radial profiles and gradients for the first 62 active galactic nuclei (AGN) observed with Sloan Digital Sky Survey (SDSS)-IV Mapping Nearby Galaxies at Apache Point Observatory (MaNGA) to study the effects of the active nuclei on the star formation history of the host galaxies. These results, derived using the STARLIGHT code, are compared with a control sample of non-active galaxies matching the properties of the AGN hosts. We find that the fraction of young SPs in high-luminosity AGN is higher in the inner ($R \leq 0.5\ R_e$) regions when compared with the control sample; low-luminosity AGN, on the other hand, present very similar fractions of young stars to the control sample hosts for the entire studied range ($1\ R_e$). The fraction of intermediate-age SP of the AGN hosts increases outwards, with a clear enhancement when compared with the control sample. The inner region of the galaxies (AGN and control galaxies) presents a dominant old SP, whose fraction decreases outwards. We also compare our results (differences between AGN and control galaxies) for the early- and late-type hosts and find no significant differences. In summary, our results suggest that the most luminous AGN seems to have been triggered by a recent supply of gas that has also triggered recent star formation ($t \leq 40\,\mathrm{Myr}$) in the central region.

Key words: galaxies: active – galaxies: star formation – galaxies: stellar content.

1 INTRODUCTION

An important galaxy evolution stage is characterized by the active galactic nuclei (AGN), a phenomenon that occurs when the galaxy's supermassive black hole (SMBH) is accreting matter from its surroundings, i.e. the accretion disc. Subsequent feedback processes start to happen, comprising radiation emitted by the hot gas in the accretion disc or by its corona, jets of relativistic particles, and winds emanating from outer regions of the disc.

Current models and simulations of gas inflows on tens to hundreds of parsec (pc) scales around galaxy nuclei lead to episodes of circumnuclear star formation (Kormendy & Ho 2013; Heckman

& Best 2014; Zubovas & Bourne 2017). Zubovas & Bourne (2017) suggest that there is a critical AGN luminosity in which the feedback of the nuclear activity increases the fragmentation of the gas clouds. Above this luminosity threshold, the feedback is powerful enough to remove the gas efficiently and stop fragmentation; for AGN luminosities under this threshold, however, the feedback is not efficient to compress the gas to high densities and enhance fragmentation. However, there is no consensus on whether AGN fuelling occurs at the same time as the star formation (Kawakatu & Wada 2008), or follows it during a post-starburst phase (Cid Fernandes et al. 2005; Davies et al. 2007, 2009) or if it is not associated with any recent star formation (Sarzi et al. 2007; Hicks et al. 2013).

A breakthrough in understanding the relation between the AGN and the surrounding stellar population (SP) can be reached by a simple, but thorough, investigation of whether young or intermediate-

★ E-mail: nicolas.mallmann@ufrgs.br

age stars are present within few hundred pc of the AGN. If the youngest stellar types are present, AGN fuelling is coeval with star formation; if instead intermediate-age stars dominate the SP, fuelling would be driven by a post-starburst, and thus the AGN phase would follow the starburst phase; finding only old stars would imply that gas inflow to the AGN is not necessarily linked to star formation.

Over the past few years, major observational effort to understand this co-evolution between AGN and the circumnuclear SP is being made using spatially resolved SP studies in large samples of galaxies (Goddard et al. 2017; Zheng et al. 2017). These studies, however, are not focused on comparing AGN hosts with non-active galaxies. One recent effort focusing on such kind of comparison was made by Sanchez et al. (2017) who found that AGN hosts are mostly morphologically early-type or early-spirals and that for a given morphology, AGN hosts are more massive, more compact, more centrally peaked, and rather pressure than rotationally supported systems when compared to the non-active galaxies. However, these studies did not use a selected control sample of galaxies to match the fundamental properties of the AGN sample, nor considered the dependence on the AGN luminosities.

This is the second paper of a series in which we aim at studying the resolved SP as well as the gas emission properties of the AGN host galaxies observed with Mapping Nearby Galaxies at Apache Point Observatory (MaNGA) and compare them with those of a control sample of non-active galaxies. In Paper I (Rembold et al. 2017), we have presented the AGN sample so far observed with MaNGA (available through the MPL-5) and have defined a control sample matching the AGN host galaxies in terms of galaxy masses, morphology, distance and inclination. In Paper I we have also characterized the SP properties of the AGN hosts as compared with those of the control sample for the single aperture SDSS-III spectrum that covers the inner 3 acrsec diameter nuclear region, using spectral synthesis via the STARLIGHT program (Cid Fernandes et al. 2005).

Aimed at investigating the relation between the nuclear activity and the hosts' star formation history (SFH), in the present paper (Paper II), we use the MaNGA datacubes of the AGN and control sample defined in Paper I to obtain the resolved SFH and SP properties for these objects. These properties were compared between the AGN hosts and inactive galaxies in different luminosity ranges. This paper is organized as follows: brief description of the MaNGA subsample chosen for this work (Section 2); the method of SP synthesis as well as the base set of SSPs (Section 3); the results of the synthesis for the AGN and control sample (Section 4); a discussion comparing the SPs of AGN and control galaxies (Section 5) and a conclusion in Section 6.

2 DATA

The study of spatially resolved properties in galaxies was always undermined by the small sample size of past integral field spectroscopy surveys, not to mention the less numerous AGN. To address this problem, the MaNGA survey (Bundy et al. 2015) was developed to observe a large sample of nearby galaxies with integral field spectroscopy.

MaNGA is part of the fourth-generation Sloan Digital Sky Survey (SDSS IV) along with APOGEE-2 (Majewski et al. 2017) and eBOSS (Dawson et al. 2016). The survey aims to provide optical spectroscopy (3600–10400 Å) of ~10 000 nearby galaxies (with $\langle z \rangle \approx 0.03$). The observations are carried with fibre bundles of different sizes (19–127 fibres) covering a field of 12 to 32 arc-

sec in diameter. The selected sample is divided into 'primary' and 'secondary' targets, the former are observed up to 1.5 effective radius (R_e) whilst the latter is observed up to 2.5 R_e. For more details, see Drory et al. (2015), Law et al. (2015) and Yan et al. (2015, 2016).

The data used in the present work are a sub-sample of MaNGA data (Law et al. 2016, MPL-5's Data Reduction Pipeline, DRP) selected in Paper I. In short, the AGN were selected from the MaNGA sample by cross-matching them with SDSS-III data products, using then the BPT diagram [OIII]/Hβ versus [NII]/Hα (Baldwin, Phillips & Terlevich 1981) to select the AGN. In addition, we have used the WHAN diagram (Cid Fernandes et al. 2010; Cid Fernandes et al. 2011) to eliminate from the AGN sample the 'LIERs', or 'fake AGN'. The resulting AGN sample contains 62 objects. To study the relationship between AGN and the SPs of the host, we have chosen two control galaxies to match each of the selected AGN hosts. The matching was done according to the morphology (using concentration and asymmetry indices), axial ratios, redshifts, galaxy inclination and total stellar masses. For more details regarding the AGN and control sample selection, see Rembold et al. (2017).

3 STELLAR POPULATION SYNTHESIS

We have used SP synthesis technique in order to derive the SFH of the galaxies of the AGN and control samples. We first briefly describe the fitting code used. We then present a summary of the data preparation and processing pipeline we have developed to manage the fitting process.
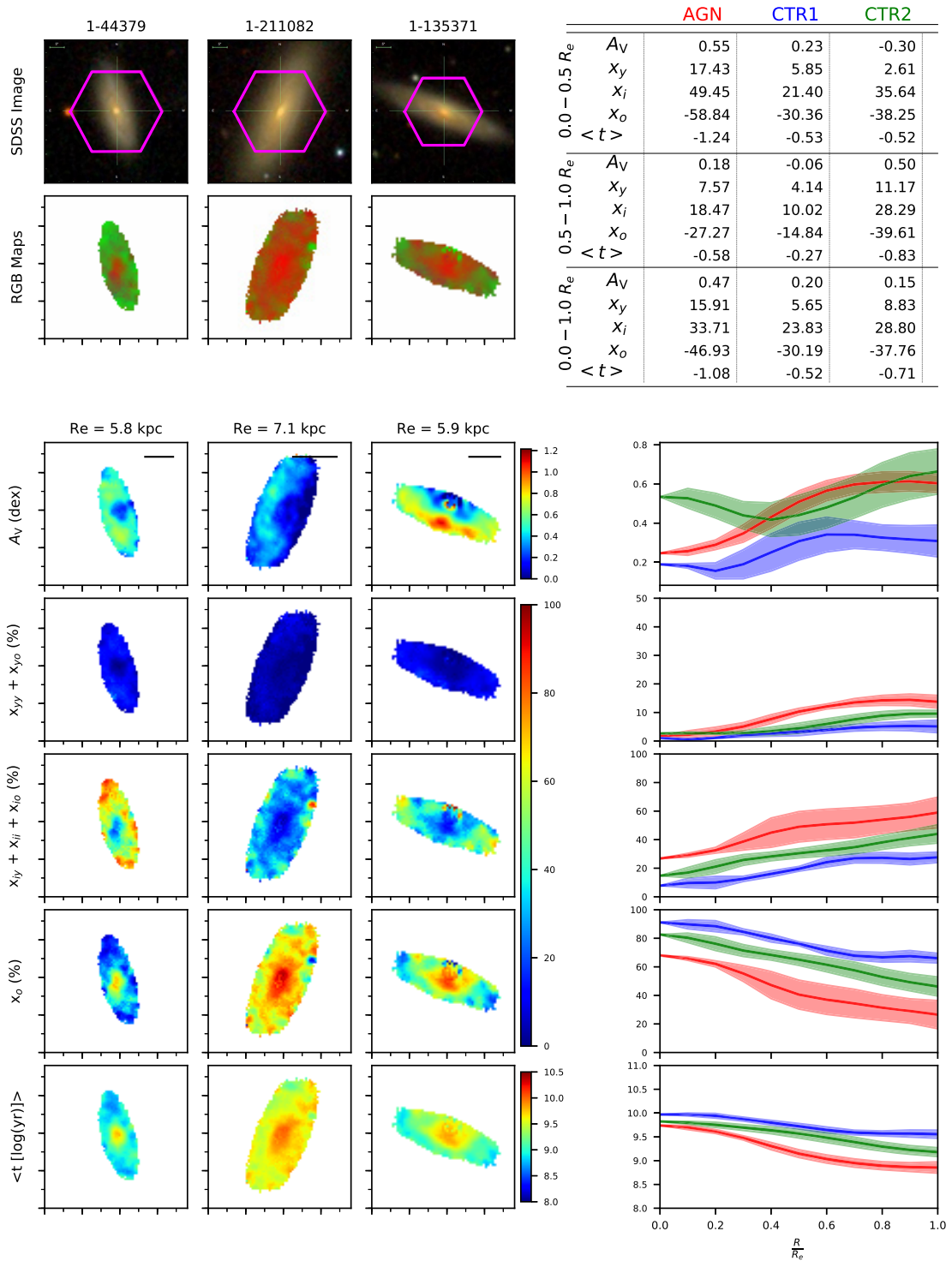
3.1 Fitting code

To disentangle the contribution of each SP to the integrated spectra of each spaxel in the datacubes we employed the STARLIGHT code (Cid Fernandes et al. 2005). In summary, this code combines the spectra of a base set of $N_\star$ template spectra $b_{j,\lambda}$ – usually, simple stellar population (SSP) covering a range of ages and metallicities – in order to reproduce the observed spectra O_λ. To generate the modelled spectra M_λ, the SSPs are normalized at an arbitrary λ_0 wavelength, reddened by the term $r_\lambda = 10^{-0.4(A_\lambda - A_{\lambda_0})}$, weighted by the population vector x_j (which represents the fractional contribution of the jth SSP to the light at the normalization wavelength λ_0), and convolved with a Gaussian distribution $G(v_\star, \sigma_\star)$ to account for the effects of velocity shifts in the central velocity $v_\star$ and velocity dispersion $\sigma_\star$. The model spectrum can be expressed as:
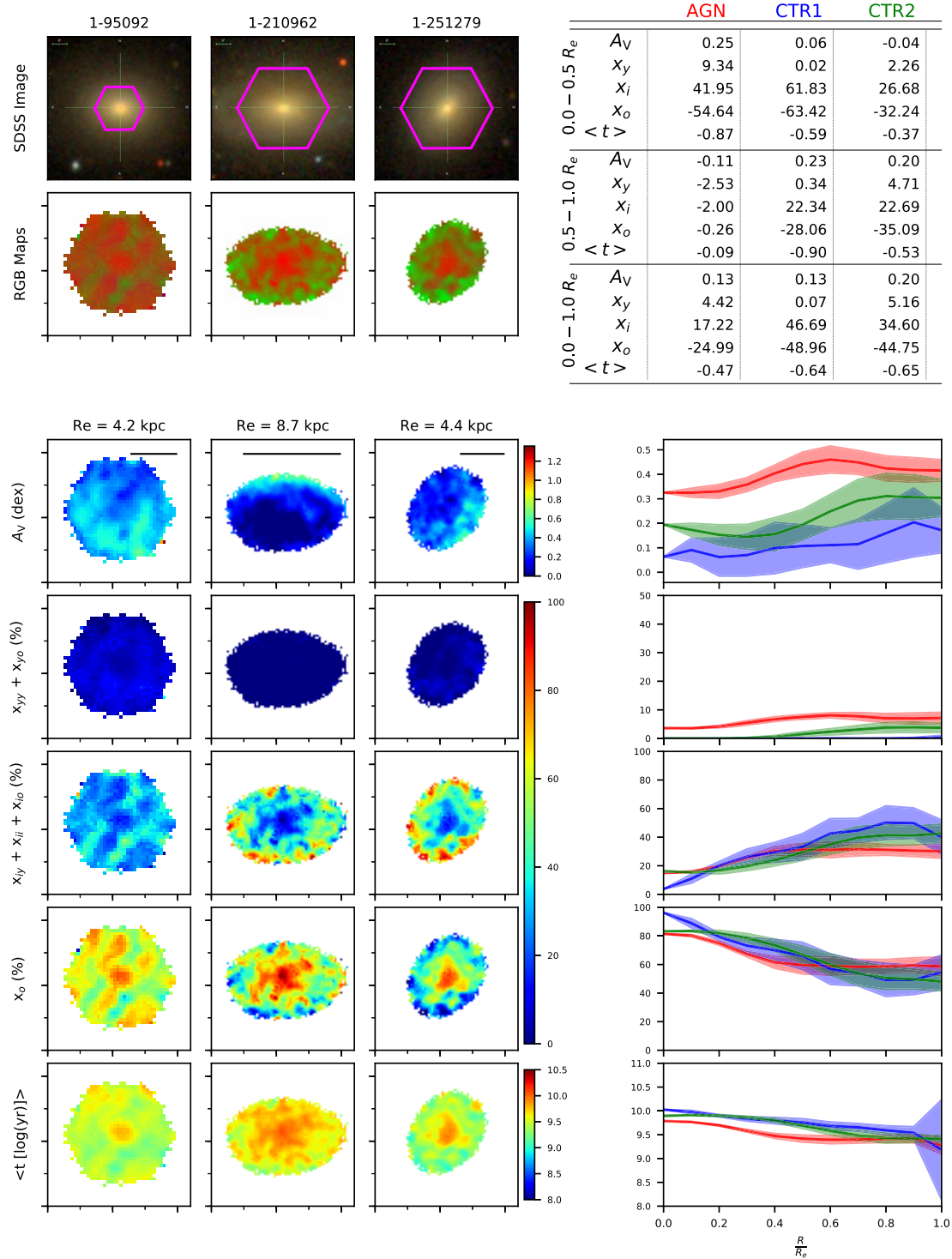
$$M_\lambda = M_{\lambda_0} \left[\sum_{n=1}^{N_\star} \mathbf{x_j}\, b_{j,\lambda}\, r_\lambda \right] \otimes G(v_\star, \sigma_\star) \tag{1}$$

where M_{λ_0} is the synthetic flux at the wavelength λ_0. To find the best parameters for the fit, the code searches for the minimum of $\chi^2 = \sum_{\lambda_i}^{\lambda_f} [(O_\lambda - M_\lambda)\omega_\lambda]^2$, where ω_λ is the inverse of the error, using a simulated annealing plus Metropolis scheme. Further details on the code can be found in Cid Fernandes et al. (2005).

The base set used in the spectral synthesis is a reduced number of the SSPs calculated by Bruzual & Charlot (2003). It comprises $N_\star = 46$ elements (45 SSPs + 1 featureless continuum – FC – function of the form $F_\nu \propto \nu^{-1.5}$ to represent the AGN emission), spanning 15 ages (0.001, 0.003, 0.005, 0.010, 0.025, 0.040, 0.101, 0.286, 0.640, 0.905, 1.43, 2.50, 5.00, 11.00 and 13.00 Gyr) and three metallicities (0.1, 1 and 2.5 $Z_\odot$). The addition of a power law

		AGN	CTR1	CTR2
0.0 – 0.5 R_e	A_V	0.55	0.23	-0.30
	x_y	17.43	5.85	2.61
	x_i	49.45	21.40	35.64
	x_o	-58.84	-30.36	-38.25
	$<t>$	-1.24	-0.53	-0.52
0.5 – 1.0 R_e	A_V	0.18	-0.06	0.50
	x_y	7.57	4.14	11.17
	x_i	18.47	10.02	28.29
	x_o	-27.27	-14.84	-39.61
	$<t>$	-0.58	-0.27	-0.83
0.0 – 1.0 R_e	A_V	0.47	0.20	0.15
	x_y	15.91	5.65	8.83
	x_i	33.71	23.83	28.80
	x_o	-46.93	-30.19	-37.76
	$<t>$	-1.08	-0.52	-0.71

Figure 1. Comparison between a late-type AGN and its control galaxies. *Left side panels – Top set of panels:* SDSS image (the MaNGA field is indicated in magenta). Second row: composed RGB image using the binned population vectors [blue: young (**X_Y**: $t \leq 40$ Myr); green: intermediate-age (**X_I**: 40 Myr $< t \leq$ 2.5 Gyr); red: old (**X_O**: $t > 2.5$ Gyr)]. *Bottom set of panels:* From top to bottom: visual extinction (A_V), **X_Y**, **X_I**, **X_O** and mean age ($<t>$) maps. For display purposes we used tick marks separated by 5 arcsec. The solid horizontal line in the A_V maps represents $1R_e$. *Right side panels – Top:* summary table with the mean gradient values for each property in three different R_e ranges. *Bottom:* average radial profiles, up to $1R_e$, for AGN (red colour) and control (blue and green colours). Shaded area represents 1σ standard deviation. For profiles smaller than $1R_e$ the gradients were calculated using extrapolated values.

		AGN	CTR1	CTR2
$0.0 - 0.5\,R_e$	A_V	0.25	0.06	-0.04
	x_y	9.34	0.02	2.26
	x_i	41.95	61.83	26.68
	x_o	-54.64	-63.42	-32.24
	$<t>$	-0.87	-0.59	-0.37
$0.5 - 1.0\,R_e$	A_V	-0.11	0.23	0.20
	x_y	-2.53	0.34	4.71
	x_i	-2.00	22.34	22.69
	x_o	-0.26	-28.06	-35.09
	$<t>$	-0.09	-0.90	-0.53
$0.0 - 1.0\,R_e$	A_V	0.13	0.13	0.20
	x_y	4.42	0.07	5.16
	x_i	17.22	46.69	34.60
	x_o	-24.99	-48.96	-44.75
	$<t>$	-0.47	-0.64	-0.65

Figure 2. Comparison between an early-type AGN and its control galaxies (see Fig. 1 for description).

is necessary to account for the AGN continuum (Cid Fernandes et al. 2004; Riffel et al. 2009). For the foreground extinction, we used the Cardelli, Clayton & Mathis (1989, CCM) law, with $R_V = 3.1$. The adopted normalization wavelength was $\lambda_0 = 5700\,\text{Å}$ and the synthesis was performed for the spectral range from 3800 to 7000 Å.

3.2 Data management

In order to improve the management of the data which include STARLIGHT inputs and outputs, the compilation of the results and the analysis, we developed a software called MEGACUBE. This software is designed to work with three main modules set up by a general
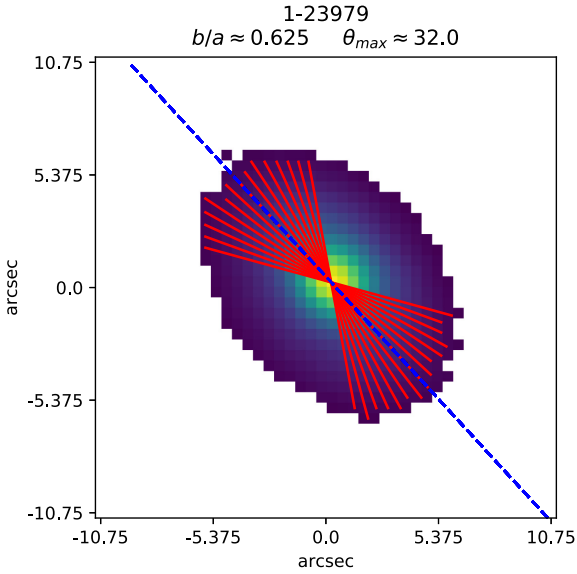
Figure 3. Example of radial profile cuts on the normalization flux map of a galaxy (MaNGA ID: 1-23979) with ≈ 32 of angle displacement from the major-axis (indicated with a blue dashed line). Red line segments are the radial profile cuts used to calculate the mean radial profile. Profiles closer to the minor axis were excluded to reduce any effects of projection (the more edge-on the galaxy is, the greater the projection distortion).

configuration file. The modular approach was chosen with adaptability in mind, e.g. if a module was programmed to work with MaNGA datacubes' extraction, we could replace it with one that extracts another survey's datacubes. The modules used in this work are (in order of execution) as follows:

i) Data preparation: This module is used to process and convert the MaNGA datacubes to a data format suitable for the chosen SP fitting code (STARLIGHT). The main steps are as follows:

(i) Filtering of the spectra using a two-dimensional butterworth filter to remove spurious data (e.g. spiked values) and increase the signal-to-noise ratio (SNR), without combining adjacent spaxel, thus allowing to a better exploration of the spatial resolution. A better description of this technique can be found in Riffel et al. (2016);

(ii) Galactic reddening correction of each spaxel using the Schlegel extinction maps (Schlegel, Finkbeiner & Davis 1998) and the CCM reddening law;

(iii) Redshift correction using the SDSS-III redshift provided in the *drpall* tables of the MaNGA database;

(iv) Estimation of the SNR in the wavelength range 5650–5750 Å for every spaxel;

(v) Spaxels with SNR < 10 were excluded when performing the fitting. This was done in order to have a good compromise between the spatial coverage and the reliability of the fitting results (see Cid Fernandes et al. 2004, for details).

ii) Spectral Fitting: This module is used to invoke the fitting code and compile its results as described below:

(i) Setting up all the configuration files needed for the fits;
(ii) Fitting each individual spaxel with STARLIGHT;
(iii) Derivation of mean ages and metallicities, as well as star formation rates, from the STARLIGHT output;
(iv) Inclusion of both standard STARLIGHT output and derived parameters to the original datacubes as additional extensions.

iii) Analysis: This module uses the fitting results to produce maps and radial plots (see Section 4 for a better description):

(i) RGB maps: qualitative representation of the spatially resolved SP age distribution for each galaxy, where the colours (red, green and blue) represent three main age bins (see Section 4);

(ii) Comparison figures: for each trio of galaxies (AGN and its two controls), panels showing the relevant properties (maps of SP properties derived from STARLIGHT and/or SDSS-III combined *ugriz* images);

(iii) Radial profiles and gradients: for each galaxy and property, a mean profile (as well as its mean gradient value – calculated as a function of R, dX/dR) is calculated to use for quantitative comparisons;

(iv) Gradients table: as a result of the analysis, we have also generated a table showing the gradients of the profiles for three different bins in terms of effective radius R_e;

(v) [O III] λ5007 luminosity $L_{[O\,III]}$binned radial profiles: radial profiles of the SP properties where the profiles for the AGN (and corresponding controls) are binned in groups according to the AGN luminosity. These profiles are shown also for AGN subsamples binned according to the host galaxy type: early- and late-type.

It is worth mentioning that a similar organizer tool was developed by de Amorim et al. (2017) for the Calar Alto Legacy Integral Field Area (CALIFA) survey, which is a pioneer project of integral field spectroscopy legacy surveys.

4 RESULTS

The spectral synthesis gives as results a number of output parameters, but we are mostly interested in x_j – the fractional contribution of each SSP to the total light at the normalization wavelength λ_0, that gives the SFH of each spaxel, and from which we also obtain the mean age for each spaxel, representing the age of the SPs as a single parameter. In addition, a valuable byproduct of the fitting is the amount of extinction in the line of sight, parameterized by the visual extinction A_V. In Figs 1 and 2 we illustrate the derived data products (maps, radial profiles and gradients) for two AGN and their respective control sample galaxies; the equivalent plots for the remaining of the sample is available in the Appendix.

In order to represent the galaxies' age distribution with a single parameter at each spaxel, we calculated their light weighted mean age (Cid Fernandes et al. 2005) as follows:

$$\langle \log t_L \rangle = \frac{\sum_{j=1}^{N_\star} x_j \log(t_j)}{\sum_{j=1}^{N_\star} x_j}, \tag{2}$$

where t_j is the age of the template j. The distributions of mean age are shown in the bottom row of the bottom left panels of Figs 1 and 2.

As stated by Cid Fernandes et al. (2005), small differences in ages of individual SSPs are washed away in real data by noise effects. We therefore rebinned the population vectors in six SP components (SPCs): x_{yy} ($1 \leq t \leq 10$ Myr), x_{yo} ($10 < t \leq 40$ Myr), x_{iy} ($40 < t \leq 286$ Myr), x_{ii} ($286 < t \leq 905$ Myr), x_{io} (905 Myr $< t \leq 2.5$ Gyr) and x_o ($2.5 < t \leq 13$ Gyr).

We have also grouped the SP vector in three major age bins, described as follows:

(i) Young Age: $X_Y = x_{yy} + x_{yo}$
(ii) Intermediate Age: $X_I = x_{iy} + x_{ii} + x_{io}$
(iii) Old Age: $X_O = x_o$
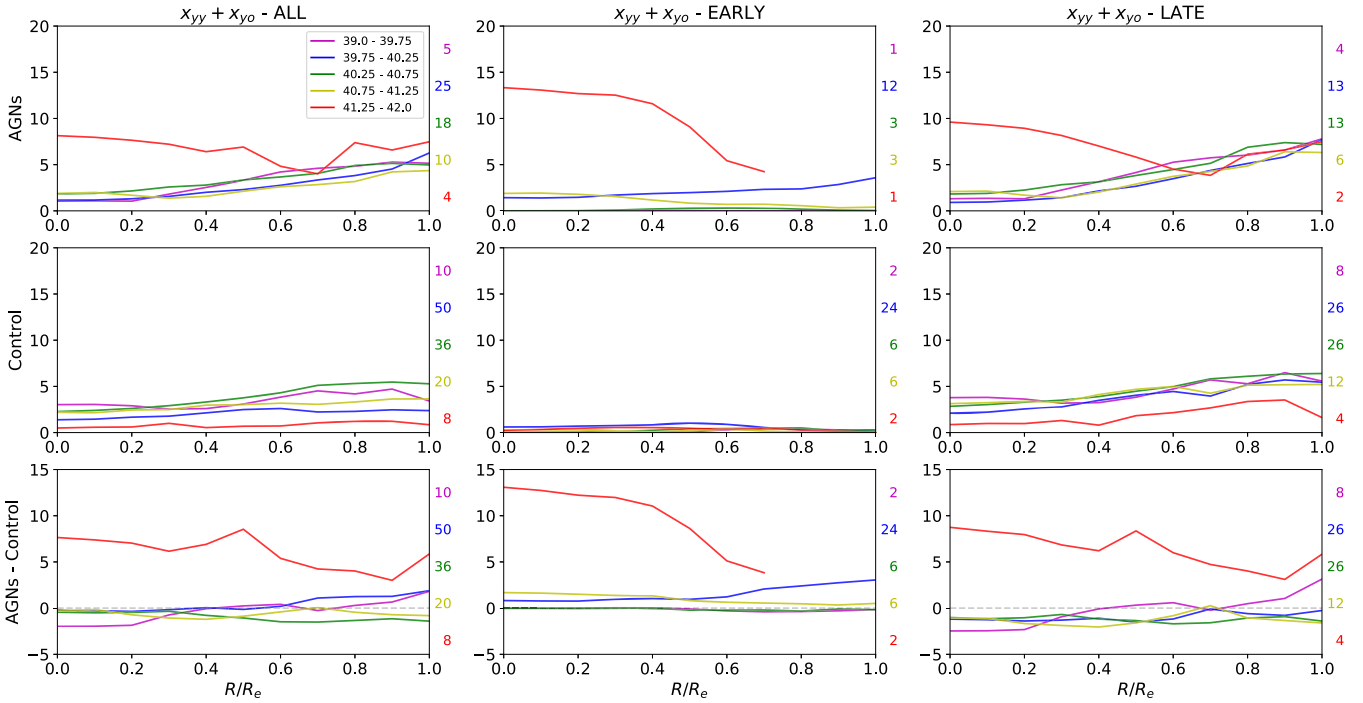
Figure 4. $L_{\text{[O\,III]}}$ binned mean radial profiles for the x_{yy} ($1 \le t \le 10\,\text{Myr}$) and x_{yo} ($10 < t \le 40\,\text{Myr}$) components combined. Each colour pertains to the same $L_{\text{[O\,III]}}$ range for every plot. The columns represent the groups of AGN used to calculate the average profiles for the AGN, its control galaxies and their differences. The groups are, from left to right: all AGN, early-type AGN, late-type AGN. The rows, from top to bottom, show the average profiles for the AGN, the control galaxies (of the respective AGN group) and the differences. The coloured numbers to the right of every plot are the quantity of galaxies used to calculate the mean profile of the same colour.
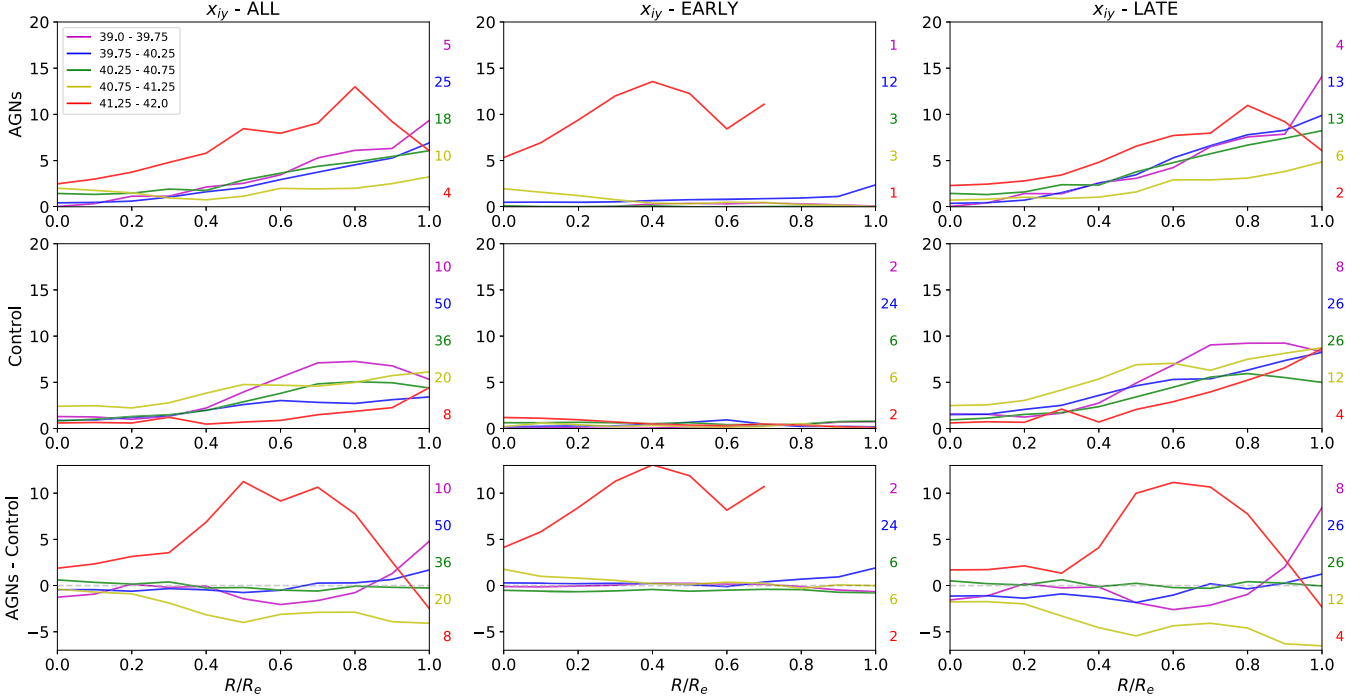
Figure 5. $L_{\text{[O\,III]}}$ binned mean radial profiles for the x_{iy} components ($40 < t \le 286\,\text{Myr}$) (see fig. 4 for description).

In order to visualize the spatial distribution of the populations' relative contributions in a qualitative way, RGB images of the galaxies were created by assigning the three colours (red, green and blue) to the binned population vectors: Red represents the old $\mathbf{X_O}$ ($2.5 <$ $t \le 13\,\text{Gyr}$), green the intermediate-age $\mathbf{X_I}$ ($40\,\text{Myr} < t \le 2.6\,\text{Gyr}$) and blue the young SPs $\mathbf{X_Y}$ ($1 \le t \le 40\,\text{Myr}$).

In the bottom right of Figs 1 and 2 we show mean radial profiles, up to $1.0\,R_e$, for each galaxy and property, derived using a
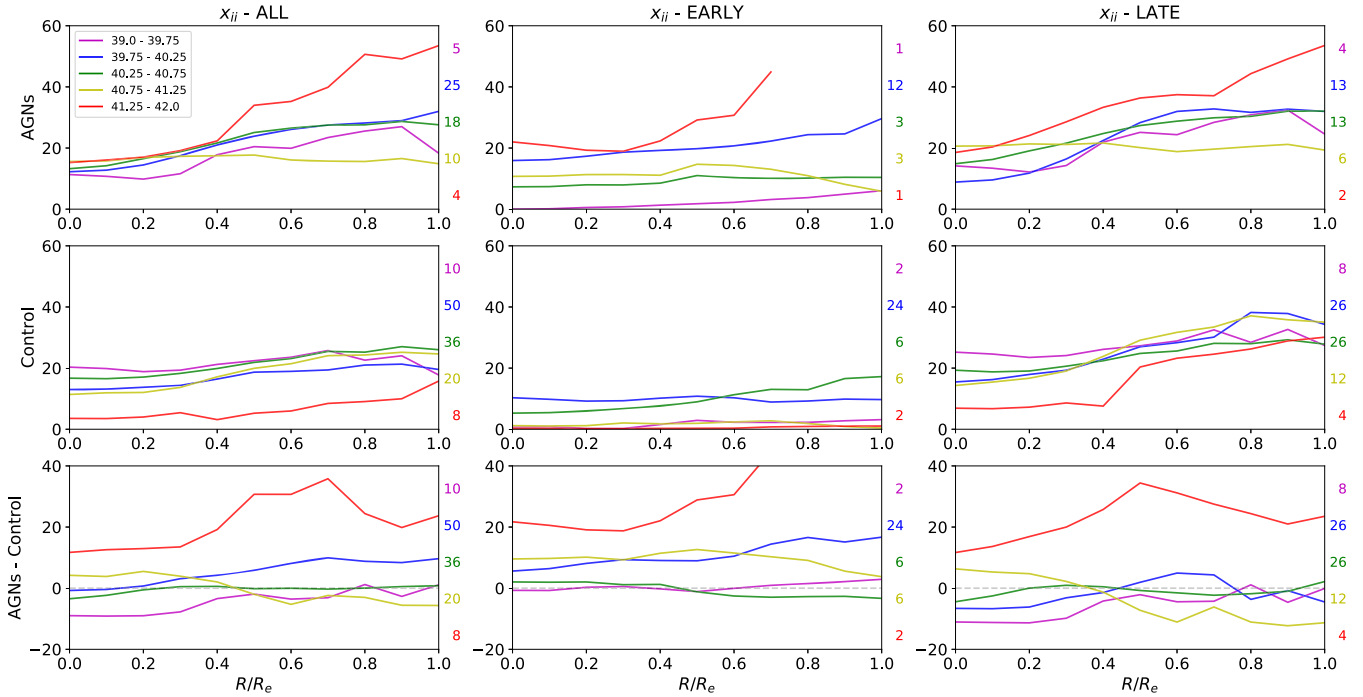
Figure 6. $L_{\rm [O\,III]}$ binned mean radial profiles for the $\mathbf{x_{ii}}$ components ($286 < t \leq 905\,\rm Myr$) (see fig. 4 for description).
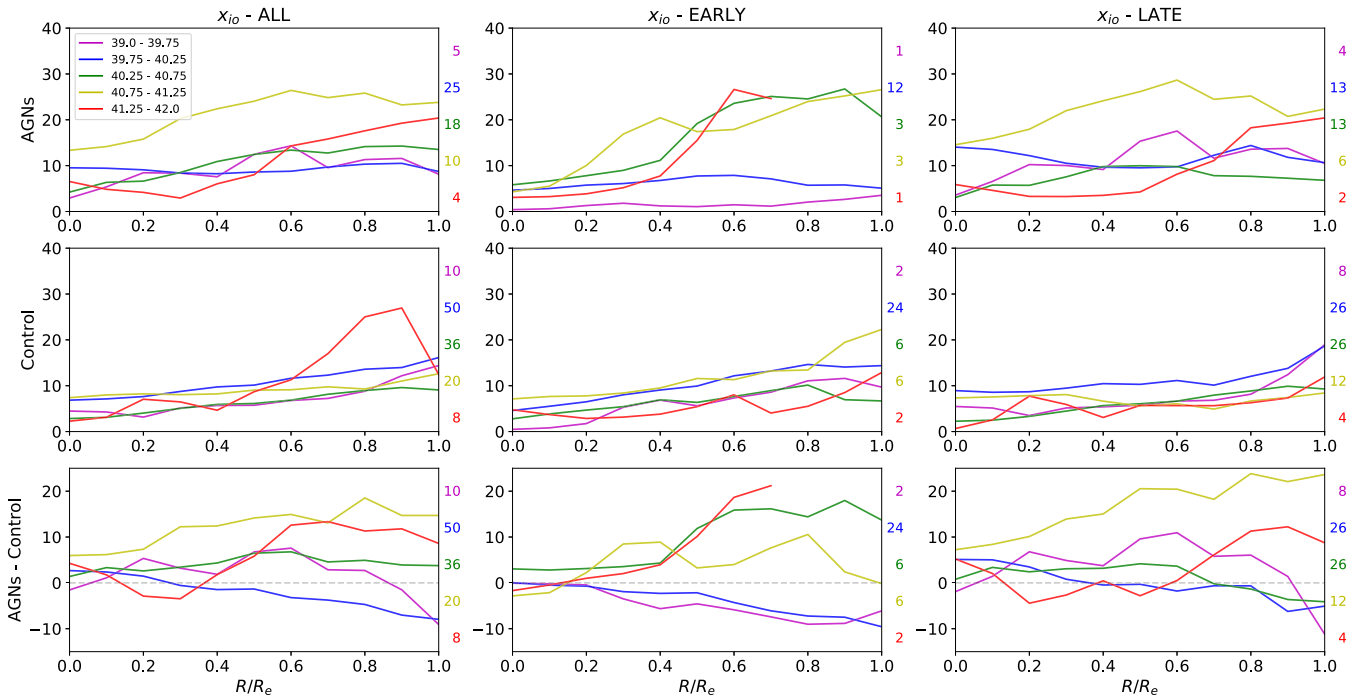
Figure 7. $L_{\rm [O\,III]}$ binned mean radial profiles for the $\mathbf{x_{io}}$ components ($905\,\rm Myr < t \leq 2.5\,\rm Gyr$) (see Fig. 4 for description).

nearest neighbor interpolation method to generate continuous values between pixel transitions and to remove abrupt changes due to spatially discrete maps. We opted for 30 equally spaced radial profiles in the galaxy plane limited to angular distances from the major axis of $\theta_{\rm max} = \tan^{-1}(b/a)$ degrees, where a and b are, respectively, the semi-major and semi-minor axis of the SDSS galaxy image, obtained from the MaNGA's *drpall* table (calculated using Sérsic profiles), as illustrated in Fig. 3. Maximum angular displacements

from the major axis were used because the profiles closer to the minor axis, when projected, resulted too noisy, possibly due to obscuration effects when the galaxies are too inclined relative to the line of sight. Mean profiles were then calculated for each property map by averaging all these profiles.

We have also calculated the mean gradients of each property (using the mean radial profiles) for three different regions: from 0.0 to $0.5\,R_{\rm e}$, 0.5 to $1.0\,R_{\rm e}$ and 0.0 to $1.0\,R_{\rm e}$. Since we are comparing rela-
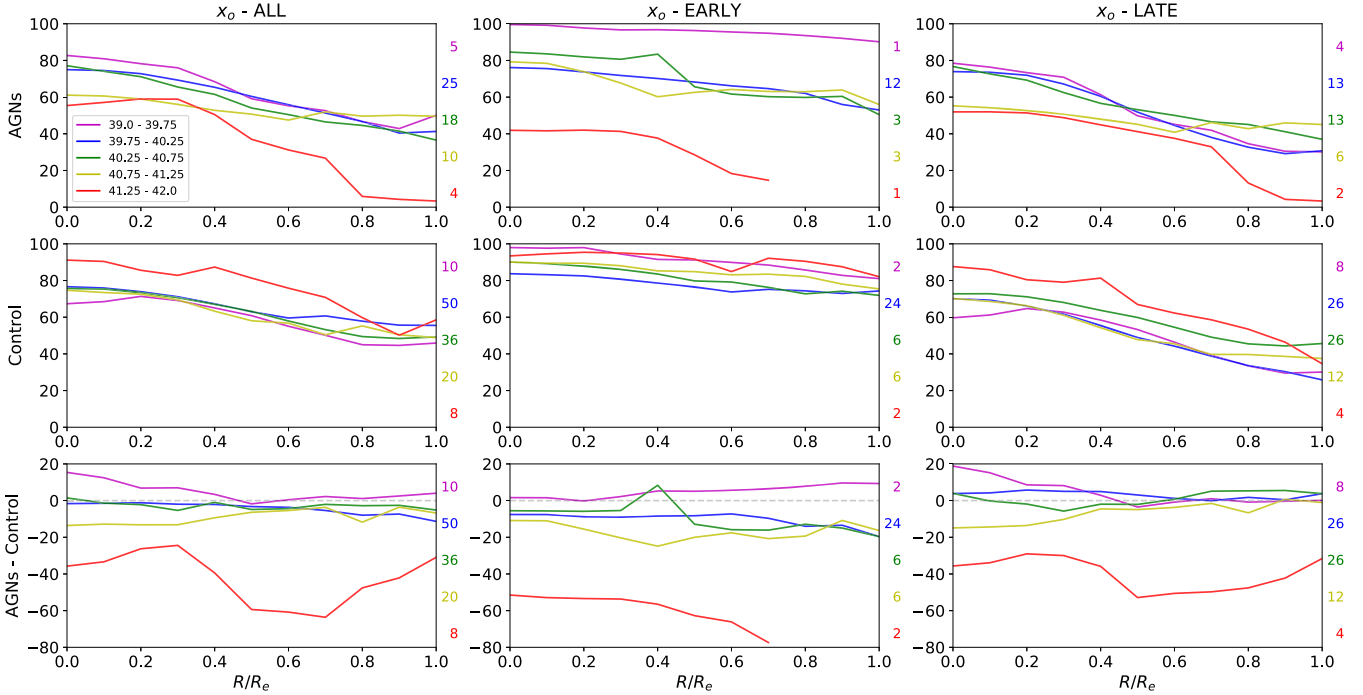
Figure 8. $L_{[O\,III]}$ binned mean radial profiles for the x_o components ($2.5 < t \leq 13$ Gyr) (see Fig. 4 for description).
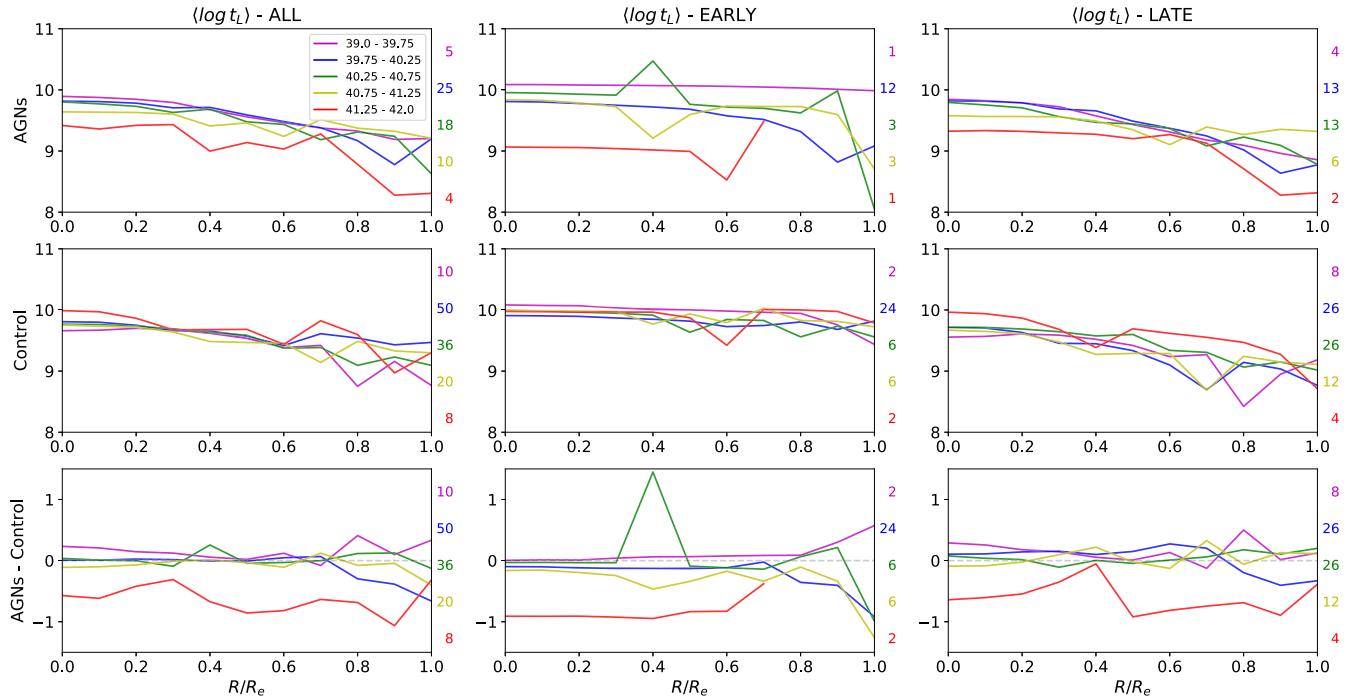
Figure 9. $L_{[O\,III]}$ binned mean radial profiles for the *mean age* ($\langle \log t \rangle$) (see Fig. 4 for description).

tively low luminosity active galaxies with a matched control sample of non-active galaxies, the major differences should be detected in their nuclear regions. Thus, the division we used was decided based on qualitative observation of the average radial profiles, which revealed, in most galaxies, a trend of slope changes close to 0.5 R_e. Some values had to be extrapolated to a constant slope since the radial profiles could not reach 1.0 R_e due to poor SNR. These gradients for A_V, X_Y, X_I and X_O, together with the gradients in

mean age, are shown in a table in the top right corner of Figs 1 and 2.

4.1 AGN hosts *versus* control galaxies

For each one of the AGN we show the radial variation of the derived properties compared to the two control galaxies in the Appendix. As an example, we have selected to show two typical sets of results
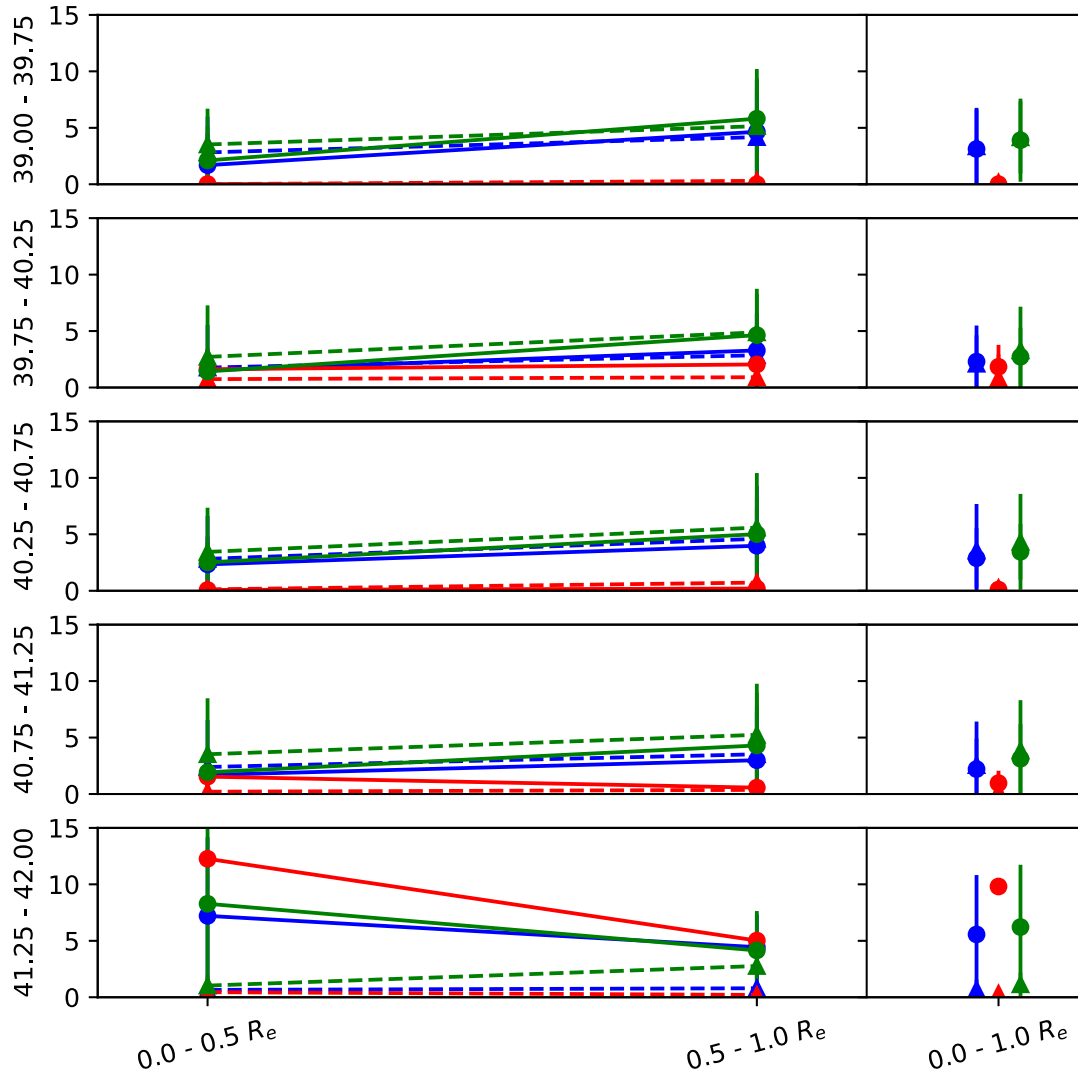
Figure 10. Young SP x_y contribution for five different bins of luminosity (39–39.75, 39.75–40.25, 40.25–40.75, 40.75–41.25, 41.25–42), calculated for three different regions (0.0–0.5 R_e, 0.5–1.0 R_e, 0.0–1.0 R_e). Each colour represents a different AGN grouping: green for the late-type AGN, red for the early-type AGN and blue for all the AGN sample. Solid lines correspond to the active galaxies and dashed lines to the control galaxies.

in Figs 1 and 2, the results for one 'late-type' AGN (MaNGA ID 1-44379) and one 'early-type' AGN (MaNGA ID 1-95092) and their control galaxies.

In the case of the late-type AGN of Fig. 1, it shows that the RGB maps are dominated by the contribution of old populations in the centres for both the AGN hosts and the control galaxies. Just outward of the nucleus, younger populations dominate the AGN and the control galaxy CRT2 a bit further out, while the control galaxy CRT1 shows larger contribution of older age components also outside the nucleus. The extinction at the nucleus is stronger for the second control than the AGN while outwards they reach similar values that are higher than those of the first control. Regarding the contribution of the different SP age bins to the light at 5700 Å, there is no difference between the AGN and the controls for the youngest age bins, while for the intermediate-age one, its contribution in the AGN is larger than in its control galaxies at all radii. There is also a difference for the old age bin X_O, that is lower in the AGN than in the control galaxies everywhere inside R_e. These results also reflect in the mean age: the mean age of the SP is lower everywhere in the galaxy for the AGN than for the control galaxies. The table listing

the gradients also shows differences between the AGN and control galaxies: for the inner radial bin (0−0.5 R_e) and for the full radial range (0−1.0 R_e), the AGN host galaxy shows steeper gradients than the controls for all properties.

The early-type AGN case of Fig. 2 shows higher contribution of the old component in the central regions of the galaxies for the AGN and its controls. In this case, however, the AGN's RGB map shows a more homogeneous population throughout the galaxy, whilst the control galaxies' RGB maps show an older central region surrounded by a younger population outwards. The extinction for the AGN is larger compared with its control galaxies as can be seen in the A_V profiles. Although the A_V maps show higher values for the control galaxies, they are concentrated closer to the limits of $SNR \leq 10$, thus less reliable. The population profiles show a more constant distribution of ages for the AGN inside the $R \leq 1.0\,R_e$, specially between 0.5 and 1.0 R_e. This behaviour is reflected in the low gradient values of the 0.5−1.0 R_e bin compared to the control galaxies. The mean age profile of the AGN shows a younger population over almost all of the 0−1.0 R_e range, similar to the late-type case (Fig. 1). The gradients table shows that the outer region
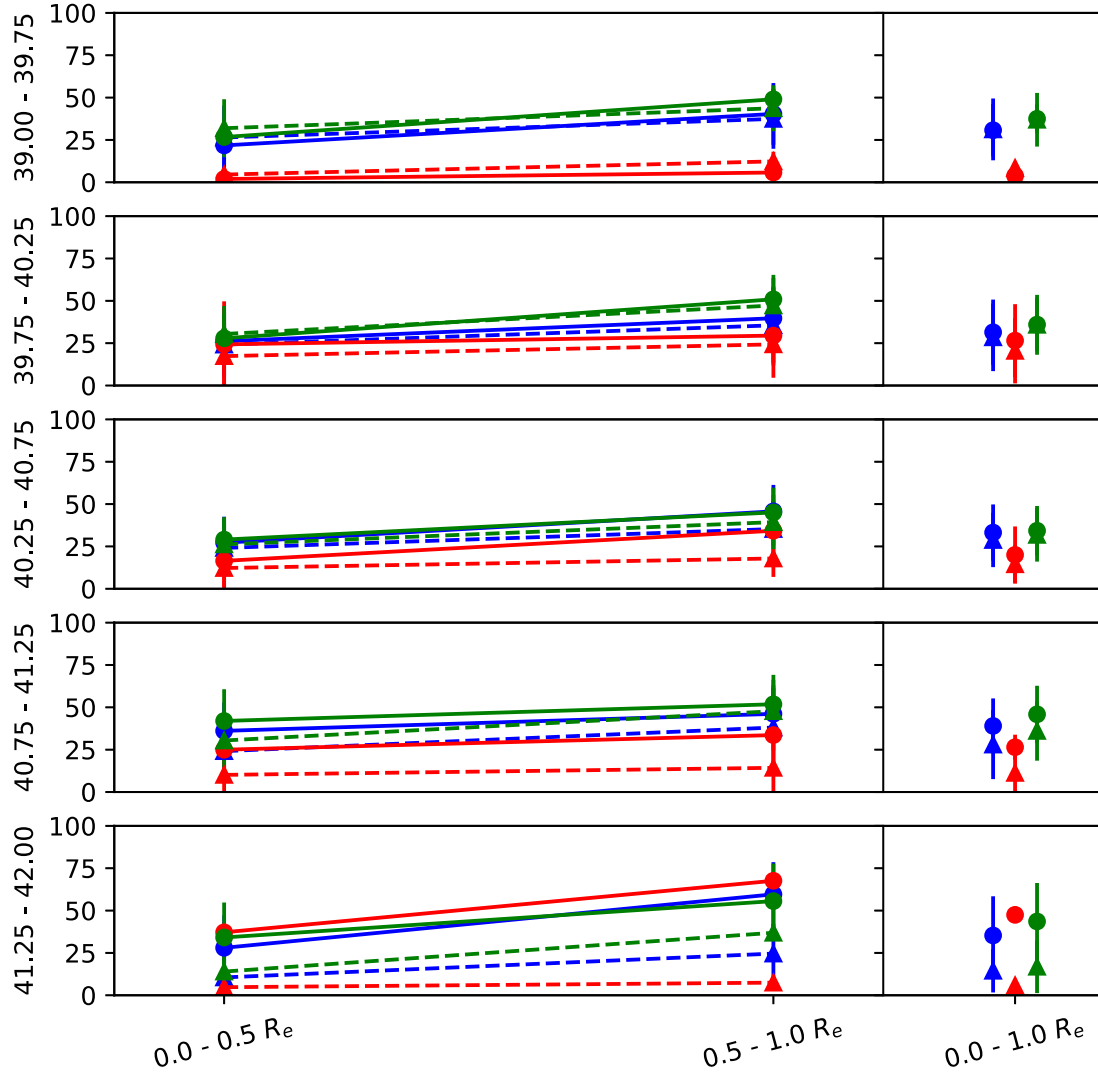
Figure 11. Intermediate-age SP x_i for different bins of luminosity, calculated for three different regions (see Fig. 10).

$(0.5 - 1.0 R_e)$ has a different behaviour for the AGN compared to the control galaxies (which, in turn, behave similarly).

5 DISCUSSION

In order to test for a possible relation between the AGN luminosity and the SFH, we compare the SP profiles derived for the AGN and controls building average profiles for each of five $L([O\,III])$ bins. We grouped them in bins of $\log_{10} L_{[O\,III]}$ as follows: 39 to 39.75, 39.75 to 40.25, 40.25 to 40.75, 40.75 to 41.25 and 41.25 to 42, using the values for $L_{[O\,III]}$ listed in Paper I.

In Figs 4 to 9 we show the mean radial profiles for the different age bins (see Section 4 as well as for the mean ages). In order to see if there are differences in these profiles for early- and late-type galaxies, we show the results for both all the galaxies grouped together and also separated in early- and late-type hosts. In the top panels we show the results for the AGN hosts, in the middle panel for the corresponding controls and in the bottom panels the difference between AGN and controls. In each panel we show the five ranges of $L_{[O\,III]}$ colour coded and the respective number of objects (coloured numbers) included in the average calculation. It

is important to note that some of the AGN are not classified as early- or late-type (because they could not be clearly classified, e.g. could be the result of mergers), so the sum of early- and late-type galaxies may not represent the total number of objects (left column).

As can be seen in Fig. 4, the clearest difference in the profiles occurs for the highest [O III] luminosity AGN, which show higher contribution of the young-age component than the controls along the whole galaxy.[1] In addition, the behaviour seems not to depend on the type of host galaxy (early- or late-type), at least up to 0.6 R_e. We note that this bin has only four galaxies, but if we look at the profiles individually, we find the same behaviour in each one of them. Comparing with the non-active galaxies, the corresponding profiles are similar to the other luminosity bins. For the late-type sources, there is a clear shift in the slope at $\sim 0.7 R_e$; for larger values of R_e it follows the other luminosity ranges. This, and the fact that the differences have a slightly negative slope in all morphology

---

[1] It is worth mentioning that we have inspected carefully the fits for the highest luminosity AGN, where differences in the young population were detected, and no problems with the synthesis quality were found.
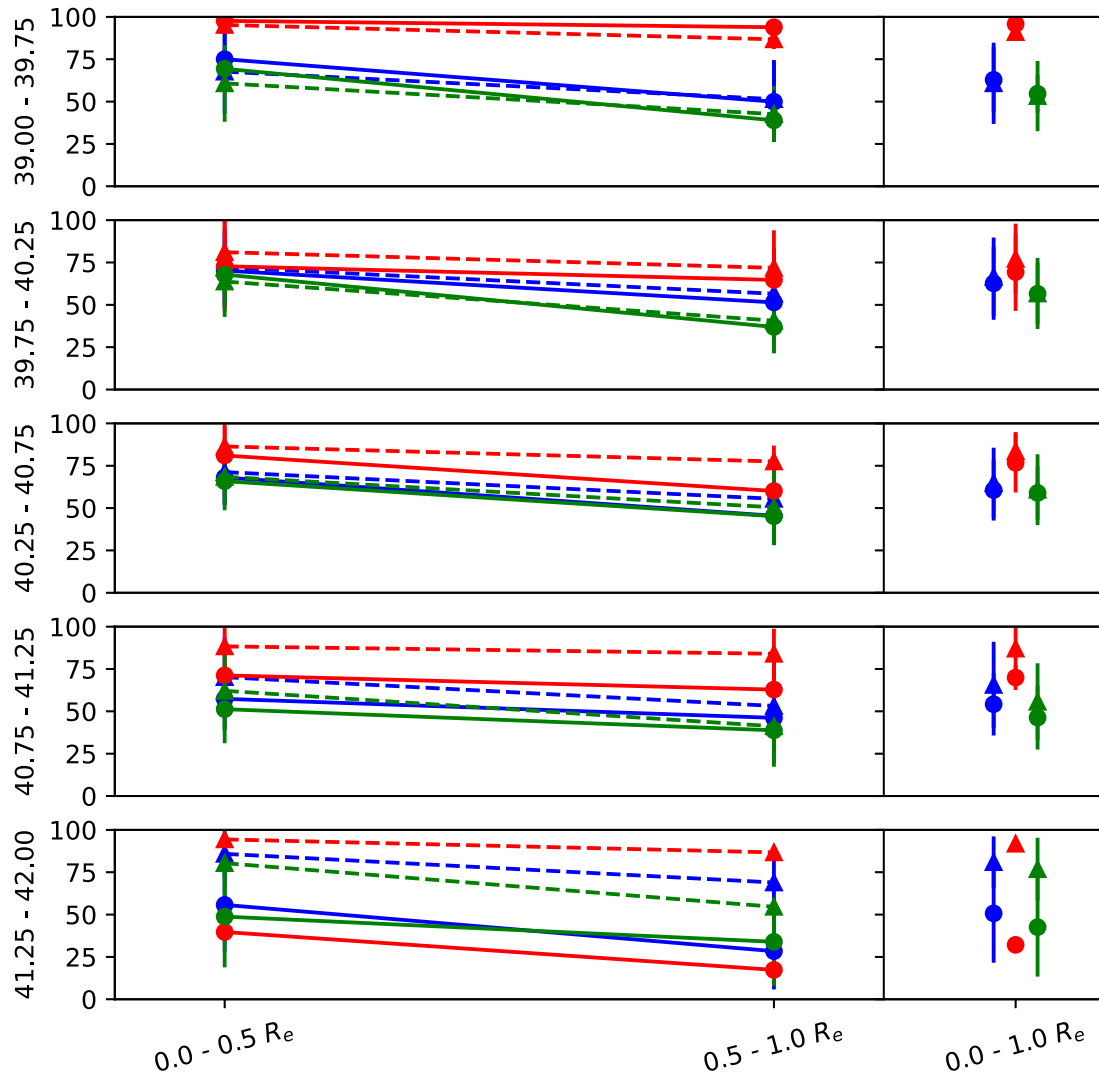
Figure 12. Old SP x_o for different bins of luminosity, calculated for three different regions (see Fig. 10).

groups, suggests that the AGN may enhance the star formation process in the nuclear region ($R_e \lesssim 0.6$).

A similar excess in the AGN as compared to controls is also observed in the intermediate-age bins x_{iy} and x_{ii} shown in Figs 5 and 6, although the excess seems to occur farther from the centre. A comparison among Figs 4–6 suggests an age stratification with radius for the highest luminosity sources, showing a larger fraction of younger stars in the central region, with the intermediate-age stars contributing more to the light in the outer regions. Regarding the old component, Fig. 7 shows that, as expected, the high-luminosity AGN has less contribution of this component than the controls, with differences ranging from ∼20 per cent to 60 per cent. A small trend can be observed also in this figure in the sense that a similar although smaller difference is also observed for the second luminosity bin, with the third and fourth bins showing almost no difference when compared with the controls, while the lowest luminosity bin showing the opposite: the controls having less contribution of the old component than the AGN.

In order to compare the galaxies using a single parameter we plot the radial profiles of their mean ages (see Section 4) in Fig. 9. It is clear from this figure that the higher luminosity AGN hosts are younger than the control galaxies in the entire studied region ($1R_e$).

We interpret these results as due to the fact that AGN hosts do prefer the 'outside-in' scenario for the recent star formation, while the galaxy's global stellar formation history (SFH) is better described by an inside-out scenario. This may reflect the idea that the active nuclei can drive the star formation process in the circumnuclear region.

Although the differences in the SP of the strongest AGN, when compared with the controls, were evident, a problem arises when trying to analyse other luminosity bins: the differences between the radial profiles are too noisy. In order to circumvent this problem, we binned the profiles into three regions (0.0–0.5 R_e, 0.5–1.0 R_e and 0.0–1.0 R_e) and the SPs into $\mathbf{X_Y}$, $\mathbf{X_I}$, $\mathbf{X_O}$. We also plotted the contribution of the FC using these radial bins to inspect the light contribution of the AGN continuum. Figs 10–14 show the results of this exercise.[2] What clearly emerges from this test is that the youngest SPs are concentrated in the inner 0.5 R_e of the most luminous AGN hosts (Fig. 10) – where the FC signature is

[2]Some galaxies have limited R_e coverage, meaning that the statistics gets weaker with radial distance. We addressed this problem by using radial intervals (0.5 R_e).
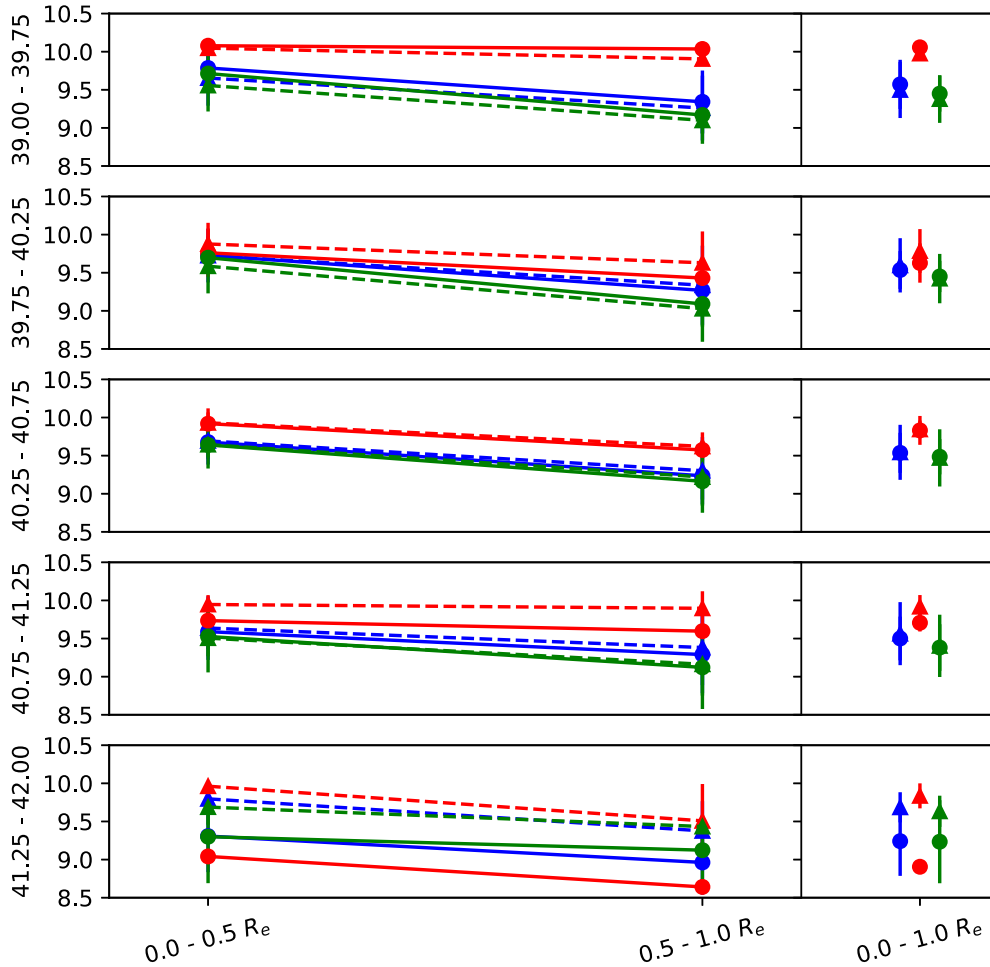
Figure 13. Mean age $\langle \log t \rangle$ for different bins of luminosity, calculated for three different regions (see Fig. 10).

the strongest (Fig. 14) – and intermediate-age ones are located in regions with radius $R \gtrsim 0.5\, R_e$ (see Fig. 11) for all AGN luminosities. In addition, the contribution of these SP components is much larger in the AGN hosts (circles) than that in the control galaxies (triangles) in the case of the highest luminosity AGN. Another result shown by these plots is that the youngest age contributions increase outwards for late-type galaxies (both controls and AGN – except the most luminous AGN).

Figs 12 and 13 show that the strongest (highest luminosity) AGN present, in general, younger SPs than their control objects. In addition these plots do allow us to better analyse the other luminosity bins. For $\log(L[\text{O\,III}])$ between 40.75 and 41.25 (the second most luminous bin) no significant differences can be seen for the younger populations, while the intermediate-age contributions are higher for the AGN, being slightly more concentrated at the outer region ($R \gtrsim 0.5\, R_e$). For the remaining luminosity bins a similar behaviour is observed, however, when looking at the overall mean values (right side of Fig. 11) it is clear that the difference vanishes with luminosity decrease.

In the case of the old SP bin, the contribution of this population in the AGN hosts is lower than that observed in the control objects, and a decrease is observed from the centre outwards. A significant difference between active and non-active sources is seen for the two highest luminosity bins, especially when using the overall mean values (right side plot). We also separate the objects according

to their Hubble types (colour coded) and no clear difference is observed between early- and late-type galaxies when comparing active and non-active hosts.

The above results reinforce literature results (Kauffmann et al. 2003; Rembold et al. 2017) in the sense that when comparing low- and high-luminosity AGN, the contribution of old SPs decreases, while that of the younger SPs increases in the latter. However, our results do additionally show that this is especially enhanced in the circumnuclear regions ($R \leq 0.5\, R_e$) indicating that the inflow of material feeding the AGN is partially being used to form stars. In addition, we suggest that these nuclear starbursts could at least be partially related to a positive AGN feedback, which may be inducing star formation in the host galaxy through enhancing the gas turbulence in the interstellar medium. Such a positive feedback is predicted by simulations (Gaibler et al. 2012; Ishibashi & Fabian 2012; Wagner, Bicknell & Umemura 2012; Zubovas et al. 2013; Bieri et al. 2015; Zubovas & Bourne 2017) and was already detected in a few objects (Cresci et al. 2015; Maiolino et al. 2017).

As can be seen from Figs 10 to 13 in general we observe that the fraction of young and intermediate-age SPs increases with the radius, while in the case of the old population, it decreases. These results support the previous findings reported by Sánchez et al. (2013), Ibarra-Medel et al. (2016) and Goddard et al. (2017) favouring an inside-out scenario for the formation of galaxies. However, when considering the most luminous AGN, it no longer applies, and it
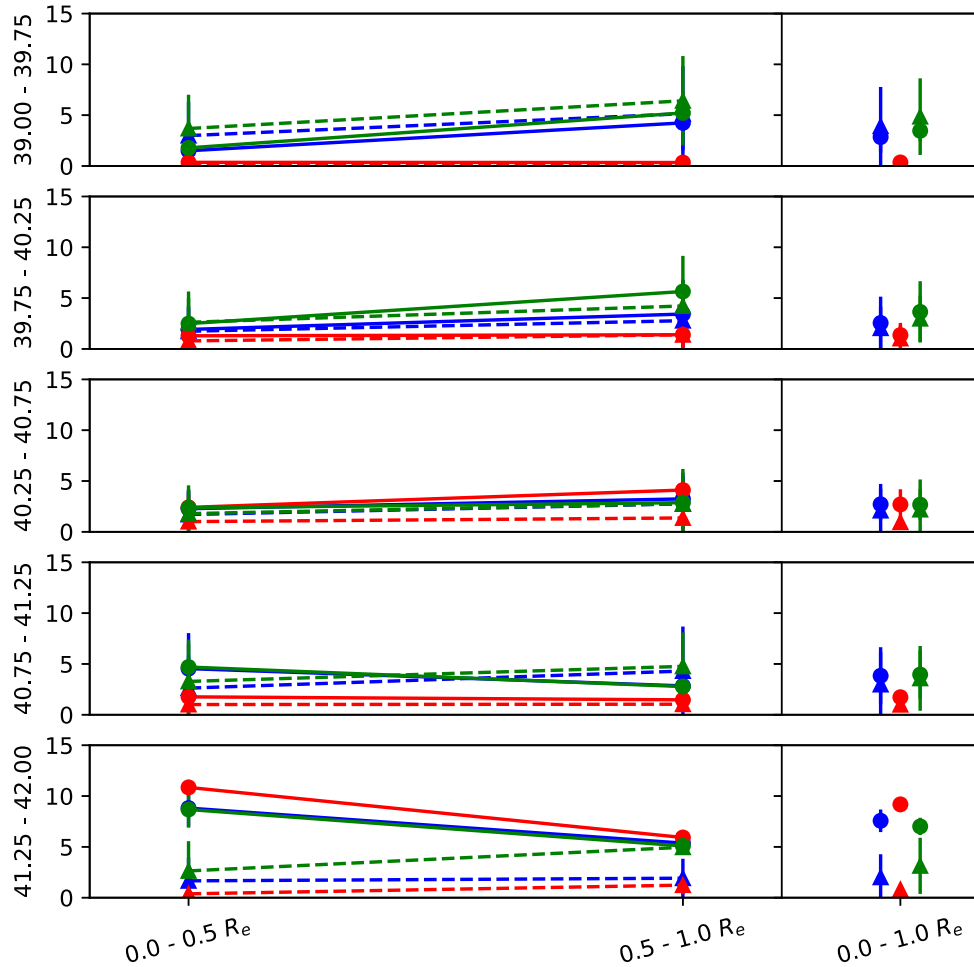
Figure 14. Featureless continuum for different bins of luminosity, calculated for three different regions (see Fig. 10).

seems that these AGN have been triggered by a recent supply of gas that has also triggered a recent star formation in their central regions. Our findings are opposite to the results of Goddard et al. (2017) in the case of early-type sources; we derive a slightly negative gradient while they derived a slightly positive one for this Hubble class.[3] On the other hand, our findings seem to agree with those of Ibarra-Medel et al. (2016), who showed that the radial stellar mass growth histories of early-type galaxies are on average nearly inside-out, though with a trend much less pronounced than that of the late-type galaxies.

6 CONCLUSIONS

We studied the stellar content of the first 62 AGN observed with SDSS-IV MaNGA and compared them with a matched sample of inactive galaxies presented in Paper I. We constructed spatially resolved SP age maps, corresponding average radial profiles and gra-

[3]Note, however, that we are studying the inner 1 R_e (they used 1.5 R_e) and a smaller sample than that studied by these authors.

dients for these sources using the STARLIGHT code, aimed at studying the effects of the AGN on the SFH of the host galaxies.

We found that the fraction of the young SP ($t \lesssim 40$ Myr) is related with the AGN luminosity. For high-luminosity AGN ($L_{[O\,III]} \gtrsim 10^{41.25}$ erg s^{-1}) it increases in the inner ($R \leq 0.5R_e$) regions when compared with the objects in the control sample. In the case of the low-luminosity AGN, both AGN and control sample hosts present very similar fractions of young stars. This result indicates that the inflow of material, besides feeding the nuclear engine, is being used to form new stars, thus rejuvenating the stellar content of the nuclear region of the AGN hosts. In addition, this very young starburst could also be enhanced by a positive AGN feedback produced by the high-luminosity AGN.

The fraction of the intermediate-age, X_I (40 Myr $<t \leq 2.6$ Gyr), SP of the AGN hosts slightly increase outwards, with a clear enhancement over the entire galaxy when compared with the control sample. In addition, our results show that the inner region of the galaxies is dominated by an old SP, whose fraction decreases outwards. These results support the previous findings of the CALIFA team (Sánchez et al. 2013), supporting an inside-out scenario for the galaxies' SFH.

We also investigated for differences on the star formation histories between the different Hubble types. No significant differences were found between early- and late-type host galaxies.

From our results we suggest that an outside-in scenario better describes the recent star formation in the AGN hosts, while an inside-out scenario represents better the older generations of stars.

REFERENCES

Baldwin J. A., Phillips M. M., Terlevich R., 1981, PASP, 93, 5
Bieri R., Dubois Y., Silk J., Mamon G. A., 2015, ApJ, 812, L36
Bruzual G., Charlot S., 2003, MNRAS, 344, 1000
Bundy K. et al., 2015, ApJ, 798, 7
Cardelli J. A., Clayton G. C., Mathis J. S., 1989, ApJ, 345, 245
Cid Fernandes R., Gu Q., Melnick J., Terlevich E., Terlevich R., Kunth D., Rodrigues Lacerda R., Joguet B., 2004, MNRAS, 355, 273
Cid Fernandes R., Mateus A., Sodré L., Stasińska G., Gomes J. M., 2005, MNRAS, 358, 363
Cid Fernandes R., Stasińska G., Mateus A., Vale Asari N., 2011, MNRAS, 413, 1687
Cid Fernandes R., Stasińska G., Schlickmann M. S., Mateus A., Vale Asari N., Schoenell W., Sodré L., 2010, MNRAS, 403, 1036
Cresci G. et al., 2015, ApJ, 799, 82
Davies R. I., Maciejewski W., Hicks E. K. S., Tacconi L. J., Genzel R., Engel H., 2009, ApJ, 702, 114
Davies R. I., Müller Sánchez F., Genzel R., Tacconi L. J., Hicks E. K. S., Friedrich S., Sternberg A., 2007, ApJ, 671, 1388
Dawson K. S. et al., 2016, Astron. J., 151, 44
de Amorim A. L. et al., 2017, MNRAS, 471, 3727
Drory N. et al., 2015, AJ, 149, 77
Gaibler V., Khochfar S., Krause M., Silk J., 2012, MNRAS, 425, 438
Goddard D. et al., 2017, MNRAS, 465, 688
Heckman T. M., Best P. N., 2014, ARA&A, 52, 589
Hicks E. K. S., Davies R. I., Maciejewski W., Emsellem E., Malkan M. A., Dumas G., Müller-Sánchez F., Rivers A., 2013, ApJ, 768, 107
Ibarra-Medel H. J. et al., 2016, MNRAS, 463, 2799
Ishibashi W., Fabian A. C., 2012, MNRAS, 427, 2998
Kauffmann G. et al., 2003, MNRAS, 346, 1055
Kawakatu N., Wada K., 2008, ApJ, 681, 73
Kormendy J., Ho L. C., 2013, ARA&A, 51, 511
Law D. R. et al., 2015, AJ, 150, 19
Law D. R. et al., 2016, AJ, 152, 83
Maiolino R. et al., 2017, Nature, 544, 202
Majewski S. R. et al., 2017, AJ, 154, 94
Rembold S. B. et al., 2017, MNRAS, 472, 4382
Riffel R., Pastoriza M. G., Rodríguez-Ardila A., Bonatto C., 2009, MNRAS, 400, 273
Riffel R. A. et al., 2016, MNRAS, 461, 4192
Sanchez S. F., et al., 2017, RMxAA, 54, 217
Sarzi M., Allard E. L., Knapen J. H., Mazzuca L. M., 2007, MNRAS, 380, 949
Schlegel D. J., Finkbeiner D. P., Davis M., 1998, ApJ, 500, 525
Sánchez S. F. et al., 2013, A&A, 554, A58
Wagner A. Y., Bicknell G. V., Umemura M., 2012, ApJ, 757, 136
Yan R. et al., 2015, AJ, 151, 8
Yan R. et al., 2016, AJ, 152, 197
Zheng Z. et al., 2017, MNRAS, 465, 4572
Zubovas K., Bourne M. A., 2017, MNRAS, 468, 4956
Zubovas K., Nayakshin S., Sazonov S., Sunyaev R., 2013, MNRAS, 431, 793

SUPPORTING INFORMATION

Supplementary data are available at *MNRAS* online.

comparisons_62_agn.pdf

Please note: Oxford University Press is not responsible for the content or functionality of any supporting materials supplied by the authors. Any queries (other than missing material) should be directed to the corresponding author for the article.

APPENDIX A: AGN - CONTROL GALAXIES COMPARISON IMAGES

We present all the comparisons between AGN and its control galaxies in Figs A1–A62 online.

This paper has been typeset from a TEX/LATEX file prepared by the author.